

Adsorption of DNA Oligonucleotides by Self-assembled Metalloporphyrin Nanomaterials

Jinghan Wang^{1,2}, Zhen Wang¹, Po-Jung Jimmy Huang¹, Feng Bai^{*2}, Juewen Liu^{*1}

¹Department of Chemistry, Waterloo Institute for Nanotechnology, Waterloo, Ontario, Canada N2L 3G1

²Key Laboratory for Special Functional Materials of Ministry of Education, National & Local Joint Engineering Research Center for High-efficiency Display and Lighting Technology, School of Materials Science and Engineering, and Collaborative Innovation Center of Nano Functional Materials and Applications, Henan University, Kaifeng, 475004, China

Corresponding authors.

E-mail: Feng Bai, baifengsun@126.com;

Juewen Liu, liujw@uwaterloo.ca

ABSTRACT

Porphyrin assemblies have controllable morphology, high biocompatibility and good optical properties, and were widely used in biomedical diagnosis and treatment. With the development of DNA biotechnology, combining DNA with porphyrin assemblies can broaden the biological applications of porphyrins. Porphyrin assemblies can serve as nanocarriers for DNA, although the fundamental interactions between them are not well understood. In this work, zinc meso-tetra (4-pyridyl) porphyrin (ZnTPyP) assemblies were prepared in the presence of various surfactants and at different pH, yielding a variety of aggregation forms. Among them, the hexagonal stacking form exposes more pyridine substituents, and the hydrogen bonding force between the substituents and the DNA bases allows the DNA to be quickly adsorbed on the surface of the assemblies. The effects of DNA sequence and length were systematically tested. In particular, the adsorption of duplex DNA was less efficient compared to the adsorption of single-stranded DNA. This fundamental study is useful for the further combination of DNA and porphyrin assemblies to prepare new functional hybrid nanomaterials.

Introduction

In recent years, DNA bio/nanotechnology has brought a wide range of applications in the fields of biological imaging, disease diagnosis, biosensors and drug delivery.¹⁻⁶ A key aspect is to interface DNA with nanomaterials.⁷⁻⁹ Many inorganic materials such as gold nanoparticles (AuNPs) and graphene oxide (GO) were commonly used in biosensors to detect nucleic acids or small molecules by physically adsorbing DNA and aptamer probes.¹⁰⁻¹⁸ In addition, various metal oxides and other 2D materials were also extensively studied.¹⁹⁻²¹ However, relatively few studies were performed on macromolecular organic compounds such as porphyrins.

Porphyrins have good biocompatibility, fascinating optical properties, rapid electron injection and strong light capture ability, which were widely used in the field of photodynamic therapy.²²⁻²⁴ Some DNA sequences can act as enzyme mimics to promote porphyrin metalation reactions, where metal ions such as Cu^{2+} and Zn^{2+} were inserted in porphyrin rings.²⁵⁻²⁷ In addition, hemin can bind to many G-quadruplex sequences to achieve peroxidase-like catalytic activities.²⁸⁻²⁹ Molecular porphyrins and DNA can form various binding structures as well.³⁰⁻³³

Porphyrins have a high molar extinction coefficient, might be useful for developing biosensors by quenching the fluorescence of fluorophore-labeled DNA. However, most porphyrins are highly hydrophobic and insoluble in water. Fortunately, preparation of porphyrin assemblies solves the water solubility problem of porphyrin monomers.³⁴⁻³⁷ Sun and coworkers reported a kind of iron porphyrin assemblies (FePNPs) as an effective nucleic acid fluorescent detection platform.³⁸ This research confirmed the potential of porphyrin assemblies in nucleic acids detection. We are more curious of the influence of the aggregation structure and morphology of porphyrin assemblies in the adsorption and detection of nucleic acids.

In the research on porphyrin assemblies, zinc meso-tetra (4-pyridyl) porphyrin (ZnTPyP) as a popular metalloporphyrin building block has been widely used in photocatalysis, biophototherapy and antibacterial applications.³⁹⁻⁴² ZnTPyP is easy to form assemblies with different stacking structures due to the intermolecular Zn-N coordination, whose aggregation

structures can be controlled by the type of emulsifier and pH of the solution during the assembly process. In this work, we explored the influence of zinc porphyrin assemblies with different aggregation structures on DNA adsorption, and provided a research basis for the further combination of porphyrin assemblies and DNA.

Materials and Methods

Materials. Zinc meso-tetra (4-pyridyl) porphyrin (ZnTPyP) was purchased from Frontier Scientific, Inc. All the DNA samples (see Table S1) were purchased from Integrated DNA Technologies (Coralville, IA, USA). Emulsifiers including cetyltrimethyl ammonium bromide (CTAB), myristyltrimethyl ammonium bromide (MTAB) and sodium dodecyl sulfate (SDS) were purchased from Aldrich and used without further purification. Hydrochloric acid (HCl, 1 M) and sodium hydroxide (NaOH, 1 M) solutions were also purchased from Aldrich. N-(2-hydroxyethyl) piperazine-N'-ethanesulfonic acid (HEPES) was from Mandel Scientific (Guelph, Ontario, Canada). All the solutions were prepared in Milli-Q water (resistivity of 18.2 M Ω ·cm).

Characterization. Transmission electron microscopy (TEM) was performed on a JEOL IEM 2010 with 200 kV acceleration voltage. The electronic absorption spectra were collected by an ultraviolet-visible (UV-Vis) spectrophotometer (Agilent Cary 60). The crystalline structures of all of the assemblies were characterized by X-ray diffraction (XRD, D8-ADVANCE). The zeta-potential values were measured using dynamic light scattering (DLS, Nano ZS, Malvern).

Preparation of Porphyrin Assemblies. Typically, 0.5 mL ZnTPyP solution (0.01 M ZnTPyP dissolved in 0.2 M HCl solution) was quickly injected into 9.5 mL of aqueous solution containing emulsifier (0.01 M) and NaOH with rapid stirring, and the mixed solution was continuously stirred at room temperature (25°C) for 48 h. Therefore, the concentration of ZnTPyP is 0.5 mM in the final reaction system. The formed ZnTPyP assemblies were collected at 15000 rpm and washed twice with Milli-Q water to remove excess emulsifiers and impurities. The ZnTPyP assemblies with different morphologies were all prepared following the above steps, but with different types of emulsifiers, or pH adjusted by NaOH,

or different concentrations of ZnTPyP (0.45 mL, 0.01 M ZnTPyP dissolved in 0.05 M HCl solution). The two molecular models of ZnTPyP porphyrin assemblies were derived from the Porphyrin Assemblies Molecular Configuration Database at Sandia National Laboratories (Albuquerque, NM, USA).

DNA Adsorption. 10 μ L FAM-12-mer DNA (100 nM, finally concentration 10 nM) was added into 90 μ L HEPES buffer (10 mM, pH 7.6) containing a ZnTPyP assemblies (20 μ g/mL), and incubated for 10 min at room temperature. Then, the supernatant was separated from mixed solution by centrifugation at 15000 rpm. The fluorescence intensity of supernatant containing the non-adsorbed DNA was measured (Ex: 485 nm; Em: 535 nm) using a microplate reader (Infinite F200 Pro, Tecan), and the decreased fluorescence in the supernatant was used to calculate the percentage of DNA adsorption. Changing the type of the FAM-labeled DNA including the base sequence and length was also performed. In all the experiments, the concentration of the DNA and the porphyrin assemblies and the adsorption time were kept the same. To measure DNA adsorption in different pH, the same experimental procedures were used, and the pH of the HEPES buffer was changed to 6.4, 7.6, 9.5 and 11.2. After 10 min incubation, the fluorescence intensity of the separated supernatant was measured by the microplate reader.

Adsorption after ethanol washing. 10 μ L ethanol was added into the 100 μ L aqueous solution containing the ZnTPyP assemblies (20 μ g/mL). The sample was agitated and placed for 10 min at room temperature. Then, after centrifugation, the supernatant was removed and 100 μ L HEPES buffer (10 mM, pH 7.6) containing 10 nM FAM-T₁₅ DNA was added. After 10 min, the supernatant was separated from the mixed solution by centrifugation at 15000 rpm. The fluorescence intensity of supernatant containing the non-adsorbed DNA was measured using the microplate reader. The ZnTPyP assemblies without ethanol treatment was used as the control group.

DNA desorption by urea. Following the experimental steps of DNA adsorption, the 2 μ g ZnTPyP assemblies after adsorption of FAM-12-mer DNA was washed by 100 μ L urea (4 M). Then, the fluorescence intensity of the supernatant was tested by the microplate reader.

Adsorption of single- and double-stranded DNA. First, FAM-24mer DNA was mixed with c-24mer DNA (complementary strand of the 24mer DNA) or 24mer DNA (the same sequence

as FAM-24mer but without the FAM label) at different molar ratios (1:0, 5:1, 1:1, 1:5, 1:10) in the annealing buffer (10 mM tris, 50 mM NaCl, 1 mM EDTA, pH 7.5). Subsequently, 10 μ L mixed DNA (final FAM-24-mer concentration 10 nM) was added into 90 μ L of Tris buffer (10 mM, 50 mM NaCl and 1 mM EDTA) containing ZnTPyP assemblies (0.02 mg/mL), and incubated for 10 min at room temperature. Then, the supernatants were separated after centrifugation, and the fluorescence intensity of supernatant containing the non-adsorbed FAM-24mer DNA was measured calculate DNA adsorption.

Results and Discussion

Controlling the Morphology and Stacking of ZnTPyP Assemblies by pH and Emulsifier

To study the adsorption of DNA by metalloporphyrin assemblies with different assembly structures, we chose zinc meso-tetra (4-pyridyl) porphyrin (ZnTPyP) as a building block using an acid-base neutralization method to initiate micelle confined nucleation reactions. ZnTPyP has four pyridyl groups at the outer core of porphyrin, and it can be dissolved in an acidic solution to form ZnTPyP-H₄⁴⁺ to solubilize ZnTPyP powders in water.⁴³ The self-assembly of ZnTPyP was initiated by mixing the acidic aqueous solution of ZnTPyP-H₄⁴⁺ with an alkaline emulsifier solution under vigorous stirring. When the acid-base neutralization reaction occurred, ZnTPyP changed from water soluble to water insoluble due to a loss of protons, and was encapsulated within the hydrophobic interior of the surfactant micelles. Then, the weak intermolecular interactions induced the nucleation and growth of ZnTPyP assemblies within the micelles (Figure 1a). A total of five types of ZnTPyP assemblies were synthesized by changing the type of emulsifier and pH, all of which had regular morphologies and good monodispersity (Figure 1b-g). Specifically, long nanowires (ZnNWs-6, Figure 1b), quadrangular nanorods (ZnNRs-4, Figure 1c), and hexagonal nanopillars (ZnNPs-6, Figure 1d and 1g) were obtained in CTAB, MTAB and SDS, respectively, under a similar pH (11.0~12.0). Meanwhile, by changing the pH and the concentration of ZnTPyP monomers, nanocubes (ZnNCs-4, Figure 1e) and nanosticks (ZnNSs, Figure 1f) were prepared in CTAB and MTAB, respectively.

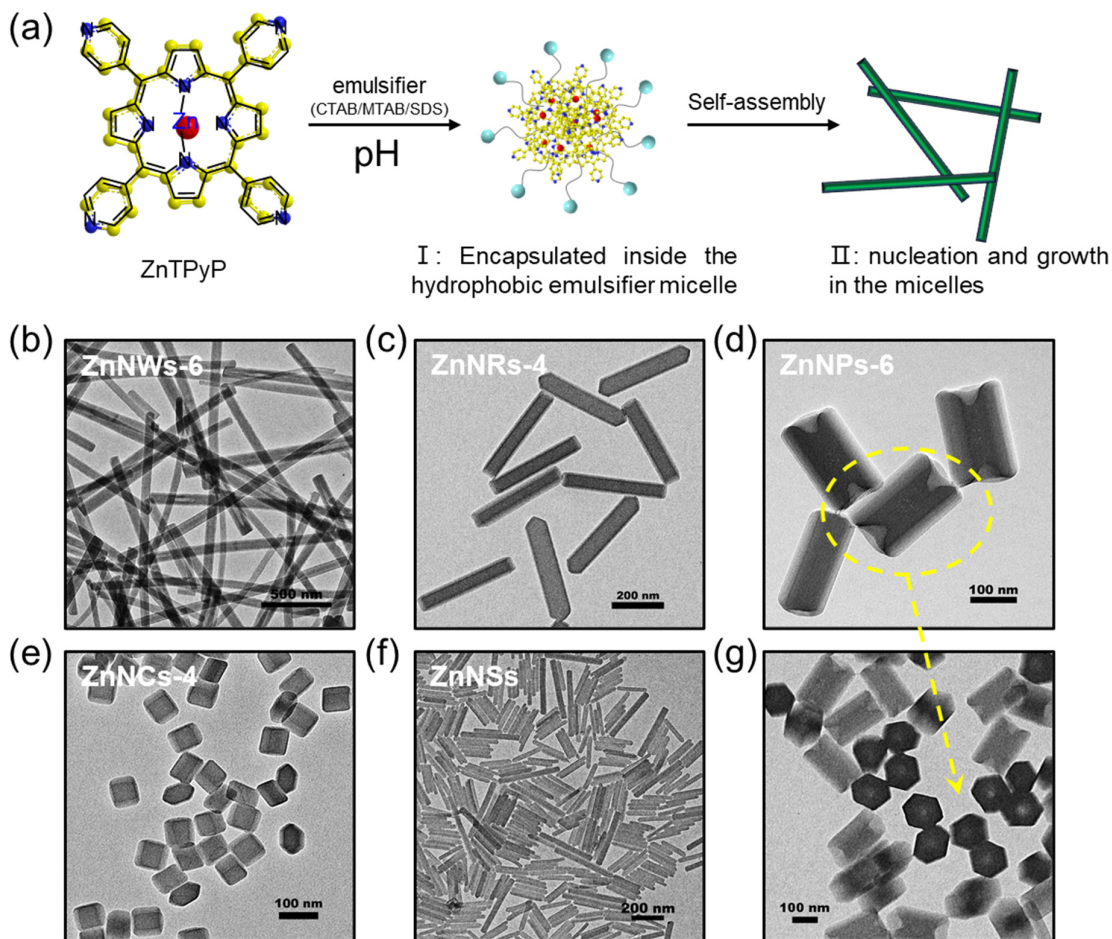


Figure 1. Preparation and morphological characterization of the ZnTPyP assemblies. (a) Schematic flow diagram of self-assembly of acid-base neutralized micelles. (b) TEM image of the ZnTPyP assemblies that were prepared using 0.5 mM ZnTPyP and 0.01 M CTAB stirring for 48 h at pH 11.7. The morphology of the ZnTPyP assemblies by changing the emulsifier to MTAB at pH 11.5 (c) and SDS at pH 11.8 (d, g) and the porphyrin concentration to 0.45 mM (e) CTAB, pH 8.4 and (f) MTAB, pH 10.9.

The change of the assembly state of ZnTPyP was reflected in the UV-vis absorption spectra. The various ZnTPyP assemblies showed split and broadened absorption peaks compared to the ZnTPyP monomers in the Q band at 443 nm (Figure 2a), suggesting the formation of J-aggregates of ZnTPyP assemblies, which resulted in a stronger exciton coupling between the ZnTPyP monomers. We further studied the molecular packing structure

of ZnTPyP with different morphologies through XRD (Figure 2b). The diffraction peaks of the ZnNWs-6 were similar to ZnNPs-6, while those of ZnNRs-4 and ZnNCs-4 were similar. However, no obvious diffraction peaks of ZnNSs were detected. Combined with our previous work on TPyP (meso-tetra (4-pyridyl) porphyrin),³⁹ we divided the crystal structure of these five ZnTPyP assemblies into three categories, including hexagonal packing (ZnNWs-6 and ZnNPs-6, Figure 2c), four-sided packing (ZnNRs-4 and ZnNCs-4, Figure 2d) and disordered packing (ZnNSs). The crystal structure of hexagonal packing based on XRD data simulation shows that each ZnTPyP molecule binds to four adjacent molecules through four identical Zn-N axis connections in forming the aggregates, two molecules at the zinc core and two at the opposite ends of the pyridyl group on the periphery, forming a hexagonal microstructure or pore channel. In addition, the four-sided stacked structure was formed through π - π stacking and ligand-to-Zn²⁺ coordination. Therefore, ZnTPyP assemblies with different structures would expose different proportions of pyridine substituents, which may have differential influences on the adsorption of DNA.

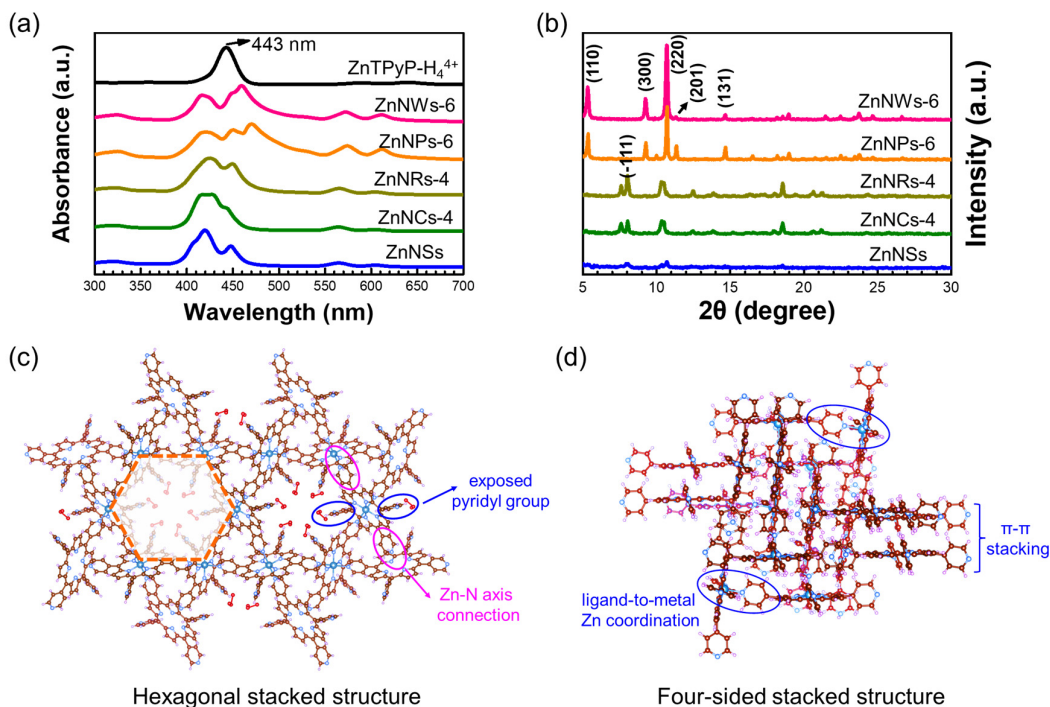


Figure 2. Characterization of the structure of the ZnTPyP assemblies. (a) UV-vis absorption spectra and (b) XRD spectra of the ZnTPyP assemblies. Simulated crystal structure of ZnTPyP assemblies with (c) hexagonal stacked and (d) four-sided stacked structures.

Surface charge, hydrogen bonding and π - π stacking directed DNA Adsorption.

To study the effect of the various ZnTPyP assemblies on DNA adsorption, a carboxyfluorescein (FAM)-labeled random-sequenced 12-mer (FAM-12mer) was used (Figure 3a). Specifically, the DNA (10 nM) was mixed with 20 μ g/mL ZnTPyP assemblies at room temperature for 10 min, and then the fluorescence in the supernatant was measured after centrifugation to calculate the DNA adsorption efficiency. At the same time, pure emulsifier solutions were also used as a control group. The results (Figure 3b) showed that the ZnTPyP assemblies of different morphologies and stacked structures exhibited different adsorption efficiencies to DNA. The DNA adsorption reached 88.2% and 36.4% for ZnNWs-6 and ZnNPs-6 with the six-sided stacked structure, while 22.3% and 94.2% for ZnNRs-4 and ZnNCs-4 with the four-sided stacking structure, respectively. In addition, the UV-vis spectra of the ZnTPyP assemblies did not change by the adsorption of DNA (Figure S1).

DNA is a polyanion, and each backbone phosphate carrying one negative charge. Although there is electrostatic interaction between the positively charged emulsifier and DNA, our control experiment showed that the emulsifier alone could not quench the FAM fluorescence (Figure S2). Therefore, the observed fluorescence decrease in the supernatants must be due to the adsorption of the DNA. It is worth noting that the zeta-potential of the ZnNPs-6 was negative by dynamic light scattering (DLS), whereas the other four ZnTPyP assemblies were all positive (Figure 3c). Since ZnNPs-6 were coated with an anionic surfactant SDS, its negative charge was understandable. All the other assemblies were prepared with cationic surfactants. Nevertheless, nearly 40% of DNA adsorption was still achieved on the surface of negative ZnNPs-6. Therefore, in addition to electrostatic interactions, other types of intermolecular forces must also be important for DNA adsorption.

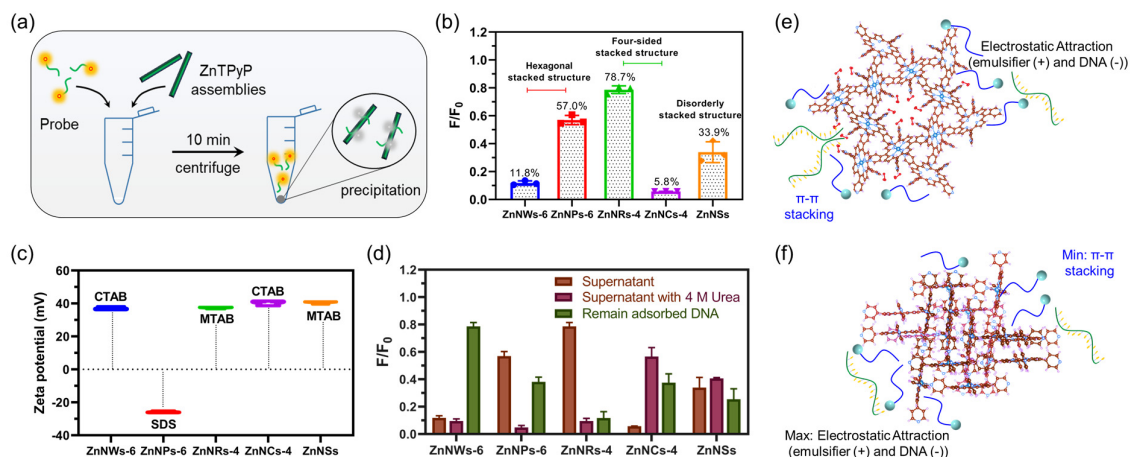


Figure 3. (a) Schematic diagram of adsorption of FAM-labeled DNA to ZnTPyP assemblies. (b) Adsorption efficiency of FAM-12 mer DNA (10 nM) on 20 $\mu\text{g/mL}$ ZnTPyP assemblies with different morphologies in HEPES buffer (10 mM, pH 7.6). (c) Zeta-Potentials of the different ZnTPyP assemblies. (d) Fluorescence intensity indicative of desorption efficiency of FAM-DNA from ZnTPyP assemblies treated with 4 M urea in HEPES buffer (10 mM, pH 7.6). Schemes showing FAM-DNA adsorption on the (e) hexagonal stacked structure or (f) four-sided stacked structure of ZnTPyP assemblies and the fluorescence change can be used to monitor the reactions.

To further understand the forces responsible for DNA adsorption, 4 M urea were used to elute the FAM-DNA pre-adsorbed on the ZnTPyP assemblies. Urea can destroy hydrogen bonding between molecules, thereby can probe potential hydrogen bonding interactions. As shown in Figure 3d, only about 10% of the DNA was eluted from the two assemblies in the hexagonal stacking, while 50-60% of the DNA was observed from the four-sided stacked structure. Therefore, hydrogen bonding was more important for the later.

Subsequently, we used computer simulation to calculate the two types of stacked porphyrin structure. The emulsifiers would be coated on the surface of the formed assemblies. However, the remaining two unconnected pyridyl groups in each ZnTPyP molecule were exposed on the pore surface in the process of forming a hexagonal packed structure, which did not exist in the four-sided packing structure (Figure 3d, e). Hydrogen bonding interactions might be generated between the pyridyl groups exposed on the surface of the

assemblies and the bases of the DNA, which causes DNA be adsorbed on the surface of the assemblies. On the other hand, the hexagonal stacked structure is more favorable for π - π stacking interactions. For the negatively charged ZnNPs-6, it had little hydrogen bonding with DNA based on our urea washing data, and we reasoned that it might adsorb the DNA via π - π stacking interactions. Porphyrins have aromatic structures and thus can stack with DNA bases.

In addition to the surface charge, hydrogen bonding, and stacking interactions, the size of the ZnTPyP assemblies might also affect the adsorption of DNA. The smallest size ZnNCs-4 with a four-sided packing structure exhibited the highest adsorption performance for the DNA. Smaller nanomaterials have a larger specific surface area, which could be helpful for DNA adsorption. In addition, for the disordered packing structure of ZnNSs, based on the large amount of DNA desorbed by urea, we reason that exposed pyridyl groups existed on the surface (to hydrogen bond with DNA). Combined with the positive surface potential, the final DNA adsorption reached 66.1%.

Effect of base, length and solution environment on DNA adsorption

Since different types of bases in DNA might have different adsorption properties to the ZnTPyP assemblies, we further explored the effect of DNA sequence using the four FAM-labeled 15mer homo-DNA. Overall, the adsorption by ZnNPs-6 and ZnNRs-4 was the lowest, regardless of the DNA sequence, and this was the same as the data collected above using the random-sequenced DNA (Figure 4a). For each ZnTPyP assembly, the C₁₅ and G₁₅ DNA appeared to be adsorbed less than A₁₅ and T₁₅. Especially, the non-adsorbed G₁₅ DNA by ZnNCs-4 was 8-fold higher than that of the other unadsorbed DNA. We reasoned that G₁₅ may fold into a G-quadruplex, which was not conducive to DNA adsorption.

Furthermore, the length of DNA was also varied using poly-A DNA. Again, the overall adsorption by ZnNPs-6 and ZnNRs-4 was lower (Figure 4b). However, the effect of DNA length was not very obvious for most assemblies, suggesting that even the very short A₅ DNA had sufficient affinity to the assemblies and the longer DNA might not use all the bases for the adsorption.

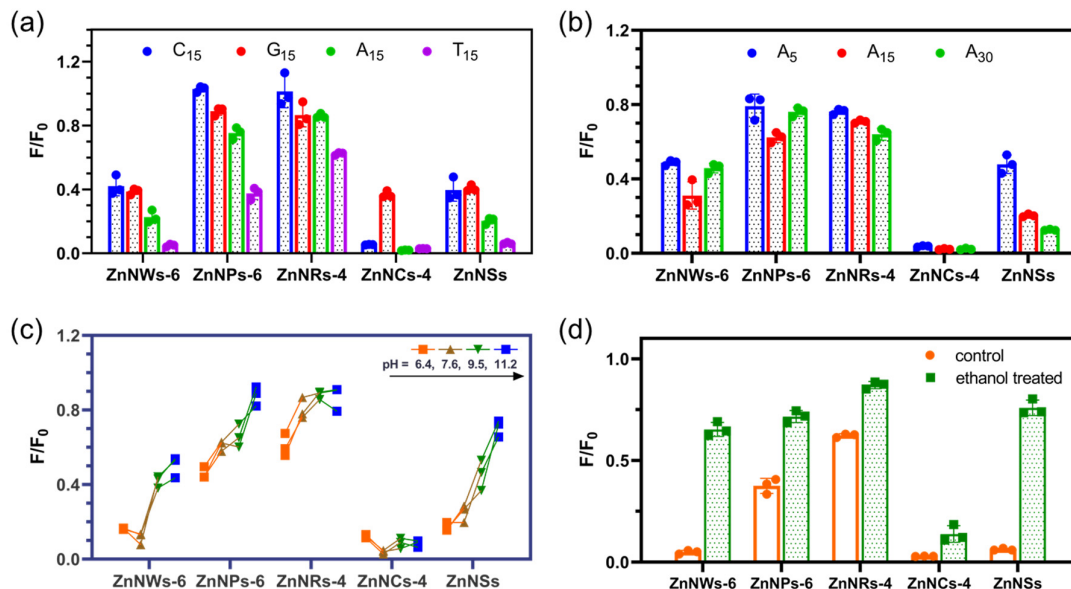


Figure 4. Effect of (a) DNA sequence (all 15-mer), (b) DNA length, (c) pH and (d) ethanol wash on DNA adsorption efficiency by the ZnTPyP assemblies in HEPES buffer (10 mM).

The pyridyl group attached to the porphine ring is a basic substituent, which can be protonated under acidic conditions to affect the adsorption of DNA. We further studied the adsorption properties of DNA under different pH conditions. The stability of the different assemblies at different pH was first studied (Figure S3). The green supernatant was observed due to disassembly at a low pH of 4.2, while for the rest pH near neutral and alkaline, all the samples had a colorless supernatant confirming stability. Therefore, we studied the effect of pH from pH 6.4 and above (Figure 4c). Among the different assemblies, ZnNCs-4 were the least sensitive to pH due to its high adsorption efficiency. For the rest, the adsorption was lower at higher pH, which can be explained by enhanced electrostatic repulsion.

In addition, the emulsifiers coated on the surface of the ZnTPyP assemblies might also affect the adsorption of DNA. Ethanol can disrupt the micelles formed by the emulsifier in water and help wash away the emulsifiers. We tested washed the ZnTPyP assemblies in an ethanol/water mixture. The washed samples were dispersed in buffer for DNA adsorption study. Taking ZnNCs-4 with the best adsorption performance as an example, the adsorption capacity of the FAM-12mer DNA gradually decreased as the concentration of ethanol

increased (Figure S4). Furthermore, we studied the adsorption of FAM-T₁₅ DNA on the surface of the ZnTPyP assemblies after washing with 10% ethanol (Figure 4d). For all the samples, the DNA adsorption decreased after ethanol treatment, suggesting that the surfactant layers were helpful for DNA adsorption. This is easy to understand for the four assemblies with cationic surfactants, and interestingly, even for the SDS-coated ZnNPs-6 assembly, washing away some SDS also decreased DNA adsorption. This might be due to the decreased colloidal stability of the samples after removing the surface protection layers.

DNA sensing on ZnTPyP assemblies

Since hydrogen bonding and π - π stacking were believed to exist between the ZnTPyP assemblies and DNA,⁴⁴⁻⁴⁵ the interaction between double-stranded DNA and the porphyrin assembly may be weakened due to shielding of the DNA bases in the duplex. Thus, the ZnTPyP assemblies might effectively distinguish between single-stranded DNA and double-stranded DNA, which could be useful for DNA detection.

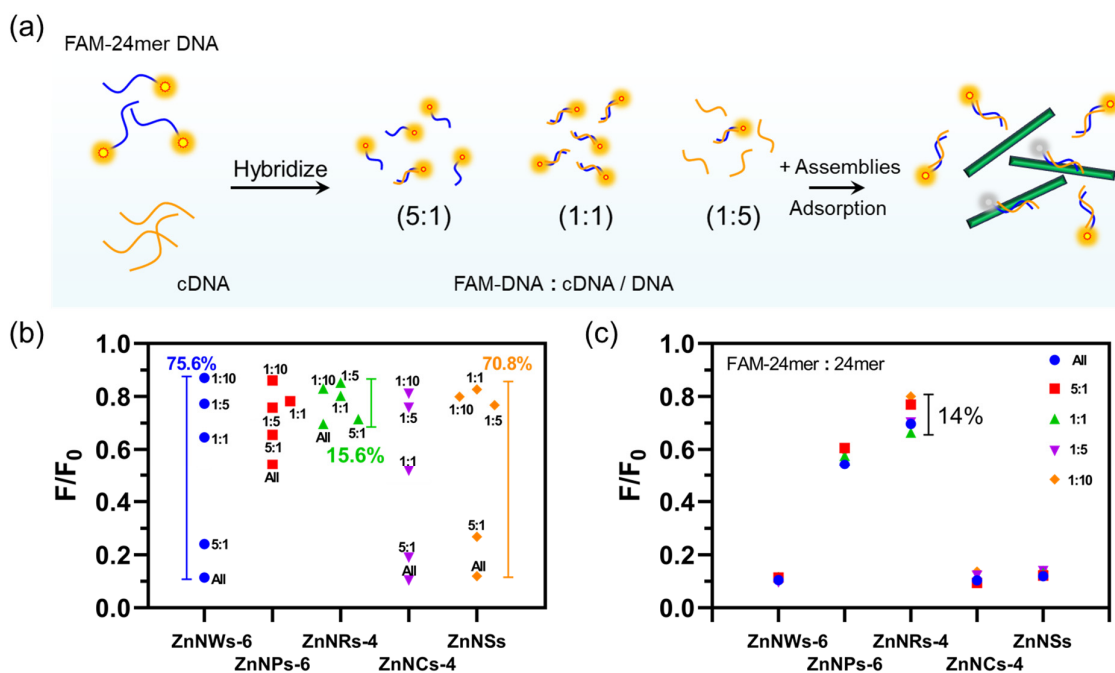


Figure 5. (a) Schematic diagram of the adsorption of FAM-DNA and cDNA duplex by ZnTPyP assemblies. (b) The fluorescence changes from different molar ratios of FAM-DNA and cDNA adsorbed on ZnTPyP assemblies in 10 mM Tris buffer (including 50 mM NaCl and 1 mM EDTA) at pH 7.5. (c) The fluorescence changes from different molar ratios of

FAM-24mer DNA and 24mer DNA (the same sequenced DNA) adsorbed on ZnTPyP assemblies.

To test the feasibility of DNA detection, we first hybridized FAM-24mer DNA with its complementary DNA (named cDNA) as shown in Figure 5a. In this process, the concentration of FAM-24mer DNA (10 nM) in the system was kept constant, and the concentration of cDNA added was adjusted from 0 to 100 nM. When only FAM-24mer DNA was added, the quenching of fluorescence was most significant, indicating the adsorption of the fluorescent probes (Figure 5b, the dots marked 'All'). Subsequently, the fluorescence intensity gradually increased with the increase of cDNA concentration, suggesting that the adsorption of the duplex DNA by the ZnTPyP assemblies was less efficient. In addition, the fluorescence became similar to that of the free FAM-24mer when a molar ratio of 1:1 was reached (FAM 24mer DNA: cDNA). Among them, the difference between single-stranded and duplex DNA reached 75.6% for the ZnNWs-6. For ZnNPs-6 and ZnNRs-4, since they were not very effective for adsorbing DNA, the effect of cDNA was the weakest. As a control, we also replaced the cDNA by the non-labeled 24mer DNA with the same sequence as the FAM-24mer. In this case, even when the molar concentration of the non-labeled 24mer was increased, the degree of DNA adsorption by the assembly hardly changed (Figure 5c). Therefore, some of the assemblies can be used to distinguish between single- and double-stranded DNA.

Conclusions

In this work, various aggregated ZnTPyP assemblies were prepared and characterized, and the adsorption of fluorescently labeled DNA oligonucleotides was achieved through a simple mixing. Among them, the ZnTPyP assemblies with a hexagonal stacking structure, especially ZnNWs-6, exposes more functional groups, allowing hydrogen bonding to facilitate DNA adsorption. Hydrogen bonding was confirmed by washing with urea. Four out of five of the assemblies were positively charged, and some DNA adsorption was observed even with the negatively charged ZnNPs-6. Therefore, other interaction forces were stronger than the charge repulsion on the surface, and adsorption can be achieved even when the surface charge

is the same as that of DNA. The effect of DNA sequence and length was overall quite moderate. On the other hand, adsorption of single-stranded DNA is much more efficient compared to the adsorption of double-stranded DNA, confirming the role of DNA bases in the adsorption process. This research provides a reference for the preparation of novel DNA/porphyrin assembly composite materials and related surface interactions.

Acknowledgements

This work was supported by the Natural Sciences and Engineering Research Council of Canada (NSERC), National Natural Science Foundation of China (Nos. 21771055, U1604139), the Zhongyuan High Level Talents Special Support Plan (No. 204200510010), the Scientific and Technological Innovation Team in University of Henan Province (No. 20IRTSTHN001). J. Wang was supported by Henan University to visit the University of Waterloo.

Supporting Information

The Supporting Information is available free of charge at <https://pubs.acs.org/doi/10.1021/acs.langmuirxxxx>

The content of the supporting information includes all DNA oligonucleotides used in this paper, the UV-vis absorption spectra of ZnTPyP assemblies before and after DNA adsorption, the fluorescence intensity changes of different emulsifiers mixed with FAM-labeled DNA, the color change picture of the supernatant of ZnTPyP assemblies with different morphologies in HEPES buffer at different pH values and the effect of ethanol on FAM-12 mer DNA adsorption efficiency of ZnNCs-4 (PDF)

References

1. Kim, H. J.; Kim, A.; Miyata, K.; Kataoka, K., Recent progress in development of siRNA delivery vehicles for cancer therapy. *Adv Drug Deliv. Rev.* **2016**, *104*, 61-77.
2. Zhang, L.; Zheng, W.; Tang, R.; Wang, N.; Zhang, W.; Jiang, X., Gene regulation with carbon-based siRNA conjugates for cancer therapy. *Biomaterials* **2016**, *104*, 269-78.

3. Li, H.; Yue, L.; Wu, M.; Wu, F., Self-assembly of methylene violet-conjugated perylene diimide with photodynamic/photothermal properties for DNA photocleavage and cancer treatment. *Colloids Surf. B. Biointerfaces* **2020**, *196*, 111351.
4. Yu, K.; Hai, X.; Yue, S.; Song, W.; Bi, S., Glutathione-activated DNA-Au nanomachine as targeted drug delivery platform for imaging-guided combinational cancer therapy. *Chem. Eng. J.* **2021**, *419*, 129535.
5. Zhang, F.; Huang, P. J.; Liu, J., Sensing adenosine and ATP by aptamers and gold nanoparticles: opposite trends of color change from domination of target adsorption instead of aptamer binding. *ACS Sens.* **2020**, *5* (9), 2885-2893.
6. Zhang, F.; Wang, S.; Liu, J., Gold nanoparticles adsorb dna and aptamer probes too strongly and a comparison with graphene oxide for biosensing. *Anal. Chem.* **2019**, *91* (22), 14743-14750.
7. Xu, W.; He, W.; Du, Z.; Zhu, L.; Huang, K.; Lu, Y.; Luo, Y., Functional nucleic acid nanomaterials: development, properties, and applications. *Angew. Chem. Int. Ed.* **2021**, *60* (13), 6890-6918.
8. Huang, J.; Su, X.; Li, Z., Metal ion detection using functional nucleic acids and nanomaterials. *Biosens. Bioelectron.* **2017**, *96*, 127-139.
9. Afonin, K. A.; Dobrovolskaia, M. A.; Church, G.; Bathe, M., Opportunities, barriers, and a strategy for overcoming translational challenges to therapeutic nucleic acid nanotechnology. *ACS Nano* **2020**, *14* (8), 9221-9227.
10. Maxwell, D. J.; Taylor, J. R.; Nie, S., Self-assembled nanoparticle probes for recognition and detection of biomolecules. *J. Am. Chem. Soc.* **2002**, *124* (32), 9606-9612.
11. Wang, W.; Satyavolu, N. S. R.; Wu, Z.; Zhang, J. R.; Zhu, J. J.; Lu, Y., Near-infrared photothermally activated DNAzyme-gold nanoshells for imaging metal ions in living cells. *Angew. Chem. Int. Ed.* **2017**, *56* (24), 6798-6802.
12. Huang, P. J.; Liu, J., Molecular beacon lighting up on graphene oxide. *Anal. Chem.* **2012**, *84* (9), 4192-8.
13. Shao, C.; Liang, J.; He, S.; Luan, T.; Yu, J.; Zhao, H.; Xu, J.; Tian, L., pH-responsive graphene oxide-DNA nanosystem for live cell imaging and detection. *Anal. Chem.* **2017**, *89* (10), 5445-5452.

14. Liu, Z.; Chen, S.; Liu, B.; Wu, J.; Zhou, Y.; He, L.; Ding, J.; Liu, J., Intracellular detection of ATP using an aptamer beacon covalently linked to graphene oxide resisting nonspecific probe displacement. *Anal. Chem.* **2014**, *86* (24), 12229-35.
15. Peng, X.; Zhu, J.; Wen, W.; Bao, T.; Zhang, X.; He, H.; Wang, S., Silver nanoclusters-assisted triple-amplified biosensor for ultrasensitive methyltransferase activity detection based on AuNPs/ERGO hybrids and hybridization chain reaction. *Biosens. Bioelectron.* **2018**, *118*, 174-180.
16. Wu, N.; Wang, K.; Wang, Y. T.; Chen, M. L.; Chen, X. W.; Yang, T.; Wang, J. H., Three-dimensional DNA nanomachine biosensor by integrating dna walker and rolling machine cascade amplification for ultrasensitive detection of cancer-related gene. *Anal. Chem.* **2020**, *92* (16), 11111-11118.
17. Zhao, Q.; Zhou, Y.; Li, Y.; Gu, W.; Zhang, Q.; Liu, J., Luminescent iridium(III) complex labeled dna for graphene oxide-based biosensors. *Anal. Chem.* **2016**, *88* (3), 1892-9.
18. Lee, J.; Yim, Y.; Kim, S.; Choi, M.-H.; Choi, B.-S.; Lee, Y.; Min, D.-H., In-depth investigation of the interaction between DNA and nano-sized graphene oxide. *Carbon* **2016**, *97*, 92-98.
19. Wang, Z.; Huang, Z.; Han, J.; Xie, G.; Liu, J., Polyvalent metal ion promoted adsorption of DNA oligonucleotides by montmorillonite. *Langmuir* **2021**, *37* (3), 1037-1044.
20. Liu, B.; Liu, J., Sensors and biosensors based on metal oxide nanomaterials. *TrAC, Trends Anal. Chem.* **2019**, *121*, 115690.
21. Zhu, C.; Zeng, Z.; Li, H.; Li, F.; Fan, C.; Zhang, H., Single-layer MoS₂-based nanoprobe for homogeneous detection of biomolecules. *J. Am. Chem. Soc.* **2013**, *135* (16), 5998-6001.
22. Ethirajan, M.; Chen, Y.; Joshi, P.; Pandey, R. K., The role of porphyrin chemistry in tumor imaging and photodynamic therapy. *Chem. Soc. Rev.* **2011**, *40* (1), 340-62.
23. Xue, X.; Lindstrom, A.; Li, Y., Porphyrin-based nanomedicines for cancer treatment. *Bioconjug Chem* **2019**, *30* (6), 1585-1603.
24. Kou, J.; Dou, D.; Yang, L., Porphyrin photosensitizers in photodynamic therapy and its applications. *Oncotarget* **2017**, *8* (46), 81591-81603.
25. Li, Y.; Sen, D., A catalytic DNA for porphyrin metallation. *Nat. Struct. Biol.* **1996**, *3* (9),

743-747.

26. Yang, H.; Zhou, Y.; Liu, J., Porphyrin metalation catalyzed by DNAzymes and nanozymes. *Inorg. Chem. Front.* **2021**, *8* (9), 2183-2199.
27. Peng, D.; Li, Y.; Huang, Z.; Liang, R. P.; Qiu, J. D.; Liu, J., Efficient DNA-catalyzed porphyrin metalation for fluorescent ratiometric Pb²⁺ detection. *Anal. Chem.* **2019**, *91* (17), 11403-11408.
28. Chinnapen, D. J. F.; Sen, D., Hemin-stimulated docking of cytochrome *c* to a hemin–DNA aptamer complex. *Biochemistry* **2002**, *41* (16), 5202-5212.
29. Li, W.; Li, Y.; Liu, Z.; Lin, B.; Yi, H.; Xu, F.; Nie, Z.; Yao, S., Insight into G-quadruplex-hemin DNAzyme/RNAzyme: adjacent adenine as the intramolecular species for remarkable enhancement of enzymatic activity. *Nucleic Acids Res.* **2016**, *44* (15), 7373-84.
30. Kumari, R.; Khan, M. I.; Bhowmick, S.; Sinha, K. K.; Das, N.; Das, P., Self-assembly of DNA-porphyrin hybrid molecules for the creation of antimicrobial nanonetwork. *J. Photochem. Photobiol B* **2017**, *172*, 28-35.
31. Scolaro, L. M.; Romeo, A.; Pasternack, R. F., Tuning porphyrin/DNA supramolecular assemblies by competitive binding. *J. Am. Chem. Soc.* **2004**, *126* (23), 7178-7179.
32. Burns, J. R.; Wood, J. W.; Stulz, E., A porphyrin-DNA chiroptical molecular ruler with base pair resolution. *Front. Chem.* **2020**, *8*, 113.
33. Börjesson, K.; Wiberg, J.; El-Sagheer, A. H.; Ljungdahl, T.; Mårtensson, J.; Brown, T.; Nordén, B.; Albinsson, B., Functionalized nanostructures: redox-active porphyrin anchors for supramolecular DNA assemblies. *ACS Nano* **2010**, *4* (9), 5037-5046.
34. He, M.; Chen, L.; Jiang, B.; Tan, H.; Wang, C.; Yang, H., Facile construction of Zn(II)-porphyrin-cored [5]rotaxane and its controllable aggregation behaviours. *Chin. Chem. Lett.* **2019**, *30* (1), 131-134.
35. Wang, S.-P.; Lin, W.; Wang, X.; Cen, T.-Y.; Xie, H.; Huang, J.; Zhu, B.-Y.; Zhang, Z.; Song, A.; Hao, J.; Wu, J.; Li, S., Controllable hierarchical self-assembly of porphyrin-derived supra-amphiphiles. *Nat. Commun.* **2019**, *10* (1), 1399.
36. Medforth, C. J.; Wang, Z.; Martin, K. E.; Song, Y.; Jacobsen, J. L.; Shelnut, J. A., Self-assembled porphyrin nanostructures. *Chem. Commun.* **2009**, 7261-7277.
37. Wang, Y.; Liu, Y.; Li, G.; Hao, J., Porphyrin-based honeycomb films and their

- antibacterial activity. *Langmuir* **2014**, *30* (22), 6419-6426.
38. Zhai, J.; Li, H.; Sun, X., A novel application of porphyrin nanoparticles as an effective fluorescent assay platform for nucleic acid detection. *RSC Adv.* **2011**, *1* (1), 36-39.
39. Wang, J.; Zhong, Y.; Wang, L.; Zhang, N.; Cao, R.; Bian, K.; Alarid, L.; Haddad, R. E.; Bai, F.; Fan, H., Morphology-controlled synthesis and metalation of porphyrin nanoparticles with enhanced photocatalytic performance. *Nano Lett.* **2016**, *16* (10), 6523-6528.
40. Wang, J.; Zhong, Y.; Wang, X.; Yang, W.; Bai, F.; Zhang, B.; Alarid, L.; Bian, K.; Fan, H., pH-dependent assembly of porphyrin-silica nanocomposites and their application in targeted photodynamic therapy. *Nano Lett.* **2017**, *17* (11), 6916-6921.
41. Wang, D.; Niu, L.; Qiao, Z. Y.; Cheng, D. B.; Wang, J.; Zhong, Y.; Bai, F.; Wang, H.; Fan, H., Synthesis of self-assembled porphyrin nanoparticle photosensitizers. *ACS Nano* **2018**, *12* (4), 3796-3803.
42. Wang, J.; Wang, Z.; Zhong, Y.; Zou, Y.; Wang, C.; Wu, H.; Lee, A.; Yang, W.; Wang, X.; Liu, Y.; Zhang, D.; Yan, J.; Hao, M.; Zheng, M.; Chung, R.; Bai, F.; Shi, B., Central metal-derived co-assembly of biomimetic GdTPP/ZnTPP porphyrin nanocomposites for enhanced dual-modal imaging-guided photodynamic therapy. *Biomaterials* **2020**, *229*, 119576.
43. Zhang, N.; Wang, L.; Wang, H.; Cao, R.; Wang, J.; Bai, F.; Fan, H., Self-assembled one-dimensional porphyrin nanostructures with enhanced photocatalytic hydrogen generation. *Nano Lett.* **2018**, *18* (1), 560-566.
44. Kushalkar, M. P.; Liu, B.; Liu, J., Promoting DNA adsorption by acids and polyvalent cations: beyond charge screening. *Langmuir* **2020**, *36* (38), 11183-11195.
45. Peng, D.; Liang, R.-P.; Qiu, J.-D.; Liu, J., Robust colorimetric detection of Cu²⁺ by excessed nucleotide coordinated nanozymes. *J. Anal. Test.* **2019**, *3* (3), 260-268.

For TOC graphics only

